Microfluid Nanofluid (2005) 1: 197–207
DOI 10.1007/s10404-004-0007-6

RESEARCH PAPER

C. Yamahata · C. Lotto · E. Al-Assaf · M. A. M. Gijs

A PMMA valveless micropump using electromagnetic actuation

Received: 7 April 2004 / Accepted: 14 June 2004 / Published online: 21 August 2004

Abstract We have fabricated and characterized a polymethylmethacrylate (PMMA) valveless micropump. The pump consists of two diffuser elements and a polydimethylsiloxane (PDMS) membrane with an integrated composite magnet made of NdFeB magnetic powder. A large-stroke membrane deflection (~200 μm) is obtained using external actuation by an electromagnet. We present a detailed analysis of the magnetic actuation force and the flow rate of the micropump. Water is pumped at flow rates of up to 400 μl/min and backpressures of up to 12 mbar. We study the frequency-dependent flow rate and determine a resonance frequency of 12 and 200 Hz for pumping of water and air, respectively. Our experiments show that the models for valveless micropumps of A. Olsson et al. (J Micromech Microeng 9:34, 1999) and L.S. Pan et al. (J Micromech Microeng 13:390, 2003) correctly predict the resonance frequency, although additional modeling of losses is necessary.

Keywords Diffuser micropump · Lab-on-a-chip · Powder blasting

1 Introduction

Since the introduction of the concept of micro total analysis systems or μTAS in 1990 (Manz et al. 1990; Manz et al. 1991), multiple fluidic microchip technologies have been developed. A continuous challenge has been the transport and pumping of small quantities of biological fluids, of the order of a few microliters per minute. The first development of a micropump dates from the 1980s with the emergence of the field of microelectromechanical systems (MEMS). Van Lintel et al. (1988) and Van de Pol and Van Lintel (1990) presented a silicon micropump based on the piezoelectric or thermopneumatic actuation of a thin membrane. Since then, other integrated silicon-based micropumps, mostly based on piezoelectric actuation, have been proposed (Nguyen et al. 2002; Tay and Choong 2002). However, for many μTAS applications, microfluidic systems need to be disposable and low-cost rendering plastic materials more competitive. Plastic micropumps have already been shown to have great potential (Olsson et al. 1998; Böhm et al. 1999; Santra et al. 2002; Nguyen and Truong 2004). Innovative methods for fluid handling were simultaneously developed, such as the use of magnetic materials for the micropump actuation. For example, magnetic liquids or ferrofluids simultaneously provide the actuation and valving functions in a micropump. A ferrofluidic actuated pipette was presented by Greivell and Hannaford (1997). Hatch et al. (2001) and Yamahata et al. (2004) reported a micropump based on the pumping and valving action of a ferrofluidic plug in a microfluidic channel. Alternatively, magnetic actuation of a membrane with integrated magnetic parts has been shown to produce large forces (a few hundred μN) and a large membrane deflection (Böhm et al. 1999; Santra et al. 2002; Zhang and Ahn 1996; Liu 1998; Khoo and Liu 2000). Such an approach combines the benefits of the strong magnetic force with the potential of external electromagnetic actuation; moreover, direct contact of the actuating element with the fluidic circuit is avoided. The use of polymer-bonded magnets directly integrated with the membrane (Lagorce et al. 1999; Santra et al. 2002; Cho and Ahn 2003) offers additional miniaturization potential. Valves are also key elements of a micropump: ball valves (Accoto et al. 2000), normally closed check valves (Nguyen and Truong 2004; Yamahata et al. 2004), valves based on the modification

C. Yamahata (✉) · C. Lotto · E. Al-Assaf · M. A. M. Gijs
Institute of Microelectronics and Microsystems,
Swiss Federal Institute of Technology Lausanne,
1015, Lausanne EPFL, Switzerland
E-mail: christophe.yamahata@epfl.ch
Tel.: +41-21-6936639
Fax: +41-21-6935950

of physical properties of liquids (Beebe et al. 2000) as well as Tesla elements (Forster et al. 1995; Morris and Forster 2003) have been proposed. A major advance in valveless pumping was demonstrated by Stemme and Stemme (1993) who substituted check valves by nozzle/diffuser elements with fluid-directing effects. Follow-up work by Olsson et al. (1995) and Olsson (1998) on the realization of in-plane nozzle/diffuser elements triggered great interest in the field of microfluidics (Gerlach et al. 1995; Gerlach 1998; Olsson et al. 1999; Nguyen and Huang 2001; Pan et al. 2003). Nozzle/diffuser micropumps are of particular interest for disposable μTAS applications because of the simple realization of the diffuser element that significantly lowers fabrication costs. Additionally, the use of the electromagnetic actuation principle, external to the pump, and the use of plastics appear to be appropriate solutions for the requirements of disposable devices.

In this paper, we describe the fabrication and characterization of an electromagnetically actuated polymethylmethacrylate (PMMA) valveless micropump. It consists of two diffuser elements and a polydimethylsiloxane (PDMS) membrane with an integrated composite magnet made of NdFeB magnetic powder. Diffuser theory is combined with numerical simulation tools to correctly dimension the micropump. Our micropump is a three-dimensional microfluidic structure consisting of four layers of PMMA, which are microstructured by powder blasting or by standard mechanical micromachining techniques. We also discuss the microfabrication of the composite magnetic membrane. A large-stroke membrane deflection (~200 μm) is obtained using external electromagnet actuation. We present a detailed analysis of the magnetic actuation force and the frequency-dependent flow rate of the micropump and analyze our experimental data using the theoretical models of Olsson et al. (1999) and Pan et al. (2003).

2 Design and theory

The pump is of the so-called "reciprocating type", which means that it uses the oscillatory movement of a membrane to displace fluids. The magnetic diaphragm-based micropump uses the reciprocating effect of a flexible, magnetic powder containing membrane in combination with two diffuser elements (see Fig. 1a). The magnetic membrane is externally actuated by an electromagnet. Diffuser elements are fluidic channel constrictions that modify the fluid dynamics such that the fluidic resistance is higher in one direction than in the other, causing the flow rate to be different in the two directions for the same applied pressure. A diffuser is characterized by a gradual widening of the fluidic cross-section in the sense of the flow and a smaller fluidic resistance. A nozzle is characterized by a gradual reduction of the fluidic cross-section in the sense of the flow and a higher fluidic resistance. In a reciprocating micropump, a nozzle/diffuser element behaves during half of the membrane actuation cycle as a diffuser, and during the other halve as a nozzle (Stemme and Stemme 1993; Olsson 1998). In the concept of the diffuser-based micropump, this directional effect is at the origin of the net pumping in an oscillating cycle because the two nozzle/diffuser elements are in a reverse orientation relative to the pumping chamber. During the "supply mode" (chamber volume increases), more fluid flows through the inlet element than through the outlet element; while during the "pump mode" (chamber volume decreases), more fluid flows through the outlet element than through the inlet element. Fig. 1b shows the geometrical parameters of a single nozzle/diffuser element. When fluidic transport is from left to right, the element acts as a diffuser, and when transport is from right to left it acts as a nozzle. In our case, the diffuser entrance has rounded corners (curvature radius $r = 100$ μm) and a width $w_1 = 100$ μm; the outlet has sharp corners and a width $w_2 = 500$ μm. The diffuser length is $L = 2.3$ mm, defining the angle $2\theta = 9.5°$. The height of the nozzle/diffuser element is $h = 250$ μm, as determined by the thickness of the PMMA sheet out of which it is microfabricated. Hence, the cross-sections of the inlet and outlet area of the diffuser are given by $A_1 = w_1 \times h = 2.5 \times 10^{-8}$ m^2 and $A_2 = w_2 \times h = 1.25 \times 10^{-7}$ m^2, respectively. The pumping

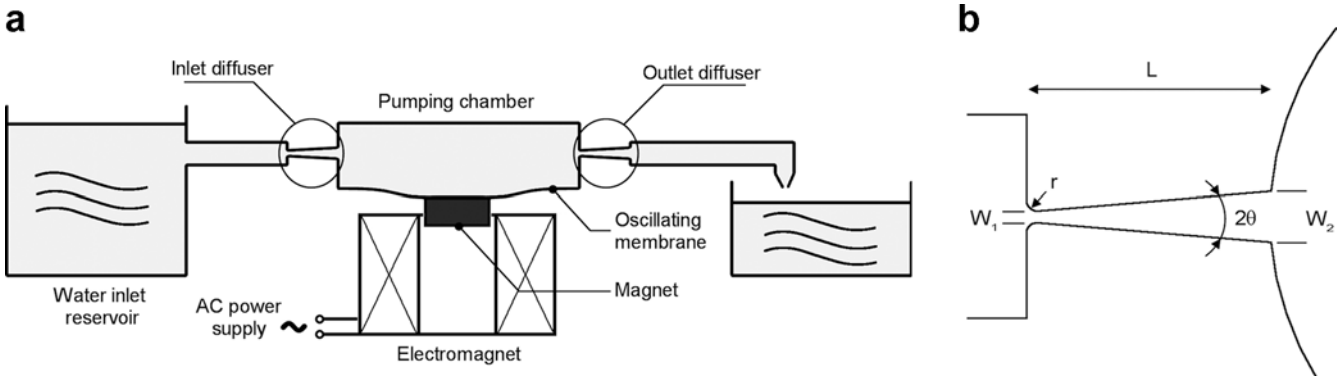

Fig. 1 **a** Schematic diagram of the diffuser micropump with external electromagnetic actuation of the magnetic membrane. The dashed area illustrates the deflection amplitude of the membrane. **b** Definition of the geometrical parameters of the diffuser element

chamber diameter is 7 mm and its depth D is 0.5 mm. Using a PDMS membrane with high deflection capabilities, we obtain a high compression ratio ϵ between the stroke volume (illustrated by the dashed area in Fig. 1a) and the dead volume of the chamber. Typically, for a membrane deflection of 200 μm, the compression ratio is $\epsilon > 0.2$. This high ϵ renders our pump self-priming and bubble tolerant (Richter et al. 1998). The large membrane deflection amplitude and the self-priming capability of our micropump are a clear advantage offered by the use of a silicone elastomer and long range magnetic actuation forces, when compared to the use of a more rigid silicon membrane with piezoelectric actuation.

An estimate of the flow-directing efficiency of the diffuser elements can be made using pressure loss data from internal flow systems. Each part of the diffuser can be treated separately and the total pressure drop can be evaluated as the sum of the pressure drop across each part. It is important to note that in the presented analytical–empirical model, one neglects (i) interferences between the different parts of the nozzle/diffuser and (ii) non-directional channel losses occurring elsewhere in the microfluidic system. Assumption (i) can be justified by the relatively large distance L between the entrance of the nozzle/diffuser element (more than 20 times the throat dimension w_1), effectively isolating each region. Assumption (ii) is for reasons of simplicity only; any experimentally found difference between theory and experiments can be related to additional channel losses. The pressure drop in an internal flow system is usually given as the loss coefficient K, which is related to the pressure drop ΔP as:

$$\Delta P = \frac{1}{2} K \rho \bar{u}^2 \tag{1}$$

where ρ is the fluid density and $\bar{u}$ is the mean flow velocity (Stemme and Stemme 1993). The loss coefficient can be found in the literature for geometries such as diverging and converging channels and sharp and rounded entrances and exits (Blevins 1984; White 1998). Figure 2 shows the dependence of the loss coefficient on the diffuser expansion angle 2θ. This graph, adapted from (Patterson 1938; Cockrell and Markland 1963), gathers from different information sources, among them being that of Gibson (1945). For diffusers with small opening angle, the losses in the diverging-wall direction are small. Gibson had estimated that for rectangular pipes with gradually diverging boundaries, minimum losses occur for a diffuser angle close to $2\theta \approx 11°$ and are associated with a loss coefficient $K \approx 0.175$ (Gibson 1945). This is the reason why we have chosen an angle close to this value for the design of our diffuser element. By considering the pressure difference over the entrance–diffuser–outlet system in terms of a normalized loss coefficient such as ξ_d

$$\Delta P = \xi_d \frac{1}{2} \rho \bar{u}_1^2 \tag{2}$$

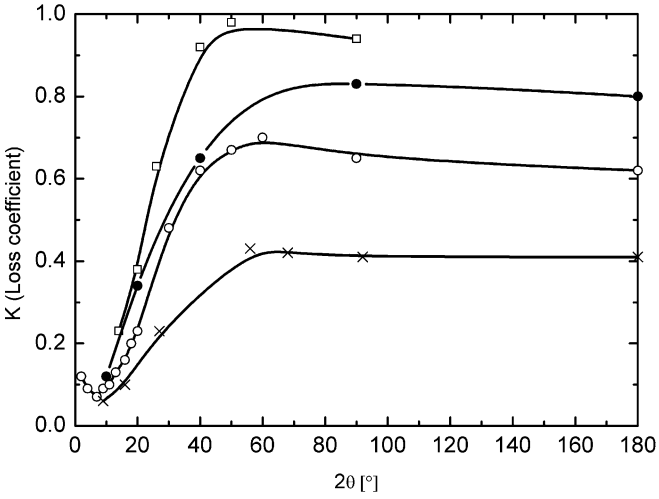

Fig. 2 Dependence of the loss coefficient for a diffuser duct combination on the diffuser expansion angle 2θ. *Open square* rectangular diffuser section with ratio of outlet to entrance area $A_2/A_1 = 9.0$; *solid circle* circular diffuser section with ratio of outlet to entrance area $A_2/A_1 = 9.0$; *open circle* circular diffuser section with ratio of outlet to entrance area $A_2/A_1 = 4.0$; *cross* circular diffuser section with ratio of outlet to entrance area $A_2/A_1 = 2.3$. Data adapted from Patterson (1938), and Cockrell and Markland (1963)

with $\bar{u}_1$ the mean velocity at the entrance of the diffuser (see Fig. 3a), one finds that (Olsson et al. 1996)

$$\xi_d = \xi_{d,e} + \xi_{d,div} + \xi_{d,o} = 0.265 \tag{3}$$

Here, we have summed the normalized loss coefficient of the diffuser ($\xi_{d,div} = K \approx 0.175$) (Gibson 1945), the normalized loss coefficient of the rounded entrance hole ($\xi_{d,e} = 0.05$) (Blevins 1984; White 1998) and the normalized loss coefficient of the outlet hole ($\xi_{d,o} = 0.04$) (Blevins 1984; Olsson et al. 1996; White 1998). When the flow is reversed the diffuser element will behave as a nozzle for which losses are completely dominated by the outlet where the cross-section is smallest. For the normalized loss coefficient of the nozzle (see Fig. 3b), one finds, analogous to Eq. 3, that

$$\xi_n = \xi_{n,e} + \xi_{n,conv} + \xi_{n,o} = 1.0 \tag{4}$$

Here, we have summed the normalized loss coefficient of the nozzle ($\xi_{n,conv} \approx 0$) (Blevins 1984; Olsson et al. 1996; White 1998), the normalized loss coefficient of the entrance hole ($\xi_{n,e} \approx 0$) (Blevins 1984; White 1998) and the normalized loss coefficient of the outlet hole ($\xi_{n,o} \approx 1.0$) (Blevins 1984; White 1998). The resulting diffuser element efficiency ratio is defined as

$$\eta = \frac{\xi_n}{\xi_d} = \left(\frac{\phi_d}{\phi_n}\right)^2 = 3.8 \tag{5}$$

with ϕ_d and ϕ_n, the volume flows in the diffuser and in the nozzle direction, respectively. The higher is η, the higher the flow-directing efficiency. This efficiency ratio is the theoretically achievable one, but is higher than the

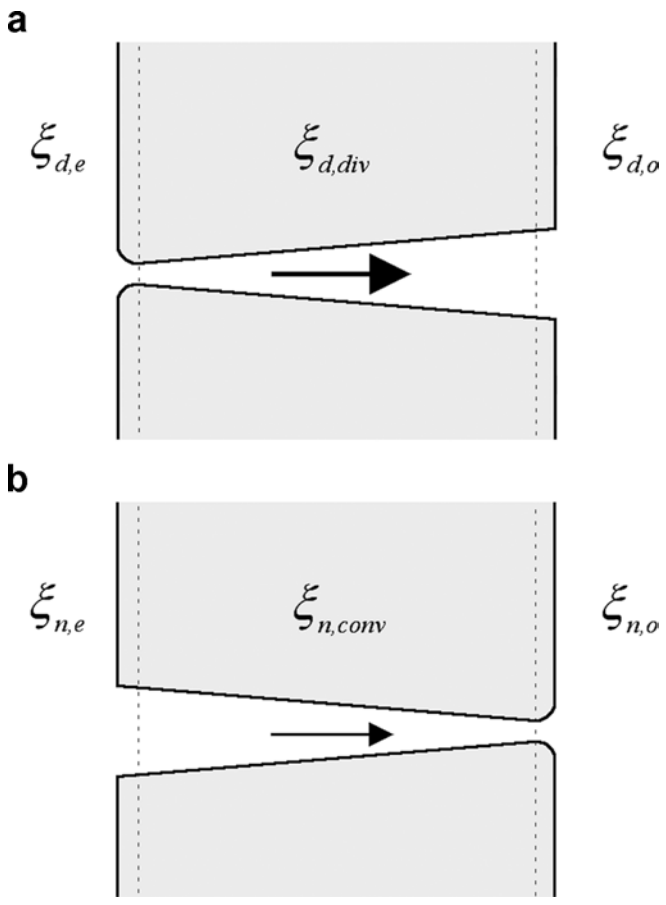

Fig. 3 Evaluation of the loss coefficients **a** in the diffuser direction and **b** in the nozzle direction

experimental parameter, as will be shown later. This may be due to flow sense independent losses in the microfluidic circuit.

3 Numerical simulation

The commercial software package Femlab 2.2 (Comsol at http://www.comsol.com/) was used to simulate the nozzle/diffuser element. The program solves the Navier–Stokes equation using a two-equation turbulence model referred to as the $k-\epsilon$ turbulence model. All simulations were done in two dimensions using water as the fluid ($\rho = 1{,}000$ kg m^{-3}; kinematic viscosity $v = 1.0 \times 10^{-6}$ m^2 s^{-1}). Defining the Reynolds number Re for a diffuser as

$$Re = \frac{\overline{u}_1 w_1}{v} \tag{6}$$

one finds that $Re = 100$ for typical flow velocities $\bar{u}_1 = 1$ m s^{-1} through the small section of the diffuser which is indicative of the development of a laminar flow regime. Singhal et al. (2004) have recently presented numerical simulations demonstrating that the flow rectification effect in nozzle/diffuser elements not only occurs in the turbulent flow regime, but can also take place for laminar flows.

Figure 4 compares the pressure distribution along the central symmetry line of a nozzle/diffuser element when flow is (a) in the diffuser direction and (b) in the nozzle direction, respectively. The simulation clearly shows that a pressure recovery effect occurs in the throat of the

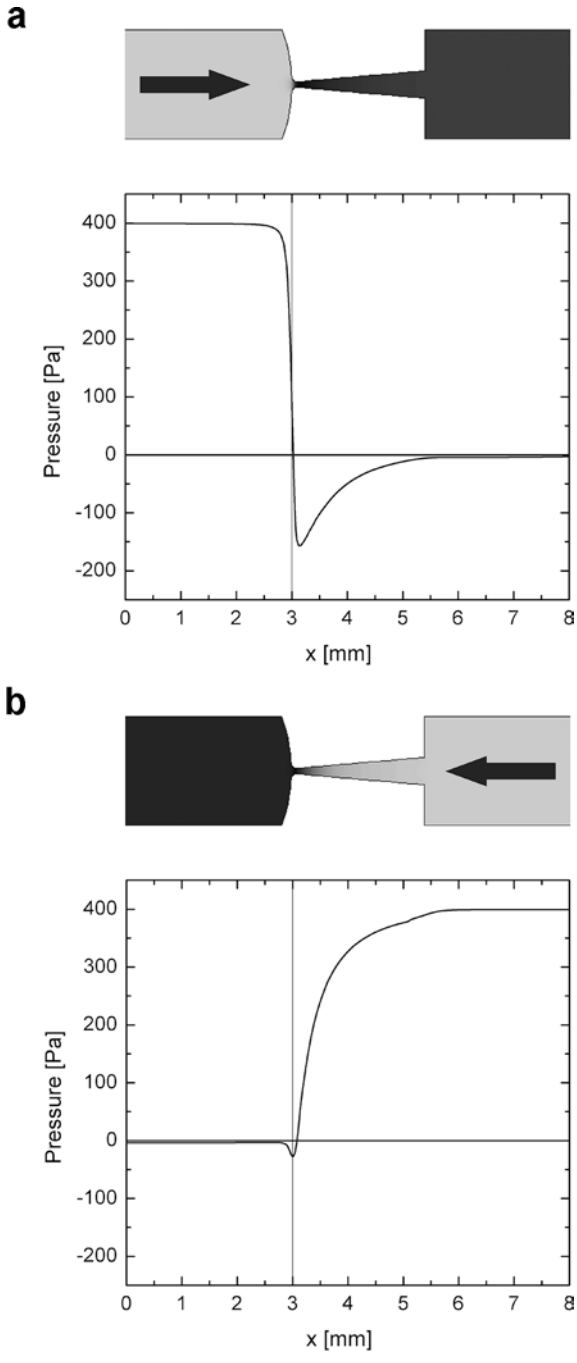

Fig. 4 Finite element simulation of the pressure distribution along the central symmetry line of **a** a diffuser element, where flow is from left to right, clearly showing the pressure recovery between the diffuser entrance and outlet and **b** a nozzle element, where flow is from right to left

nozzle/diffuser element when flow is in the diffuser direction. As was predicted by the empirical results (Patterson 1938; Gibson 1945; Cockrell and Markland 1963), this pressure recovery effect is particularly pronounced for a diffuser angle $2\theta \approx 10°$.

4 Microfabrication technology

4.1 Magnetic membrane

A NdFeB composite membrane was fabricated using a two-step molding technique. The isotropic magnetic powder MQP-S-11-9 (remanent induction: $B_r \sim 0.75$ T, Magnequench GmbH, Essen, Germany) consisting of spherical particles with a mean size of 200 μm was first mixed with commercial PDMS Sylgard 184 (Dow Corning Corp., Midland, MI, USA) to synthesize a rare-earth polymer magnet with a powder volume fraction of 40%. The membrane weight was $M_m = 0.15$ g. The effective B_r of the polymer magnet is directly correlated with the powder volume fraction, so we expect at most a $B_r \sim 0.30$ T if the magnetization is saturated. A larger PDMS membrane was integrated on top of the rare-earth magnet after degassing of the liquid PDMS in vacuum. The polymerization was achieved at 150°C during 15 min. This two-step molding procedure was made possible by the strong physical bonding between the rough surface of the polymer magnet and the larger PDMS membrane. Finally, the magnetic membrane was magnetized in an electromagnet (Magnet Charger 942 A, RFL Industries Inc., Boonton, NJ, USA), before being integrated in the PMMA chip. A photograph of a fabricated magnetic membrane is shown in Fig. 5.

4.2 Microfluidic chip

PMMA is a widely used polymer in industry and is an attractive material among plastics because of its low cost and good chemical resistance to many biochemical products. The complete pump is composed of four PMMA sheets of thicknesses 0.25 and 1.00 mm (see Fig. 6). PMMA layers were fabricated with precision milling tools (lowest layer), or using the powder blasting technique (other layers). We have recently demonstrated the potential of powder blasting for the realization of microfluidic three-dimensional structures in PMMA, using an erosion-resistive metal mask mechanically fixed on the PMMA sheet (Yamahata and Gijs 2004; Yamahata et al. 2004). Powder blasting is a rapid prototyping method and offers an efficient solution for the fabrication of fluidic devices with minimum channel dimensions in the 100 μm range. The PDMS membrane was clamped between two PMMA layers, as schematically shown in Fig. 6. During the bonding step, the four PMMA layers were assembled into a monolithic microfluidic structure using a triethylene glycol dimethacrylate solution (Fluka Chemie AG, Buchs, Switzerland). The structure was assembled in a hot press ($T = 70$°C) for only a few minutes. Figure 7a is a photograph of the final micropump including the external connectors. The external dimensions are 36 mm × 22 mm. Figure 7b shows the cross-section of a partially assembled micropump consisting of three PMMA sheets of 0.25, 0.25, and 1.00 mm thickness, respectively. A zoom on the fluidic connection of the pumping chamber with the nozzle/diffuser structure at the entrance is shown in Fig. 7c. Figure 7d shows the outlet nozzle/diffuser structure.

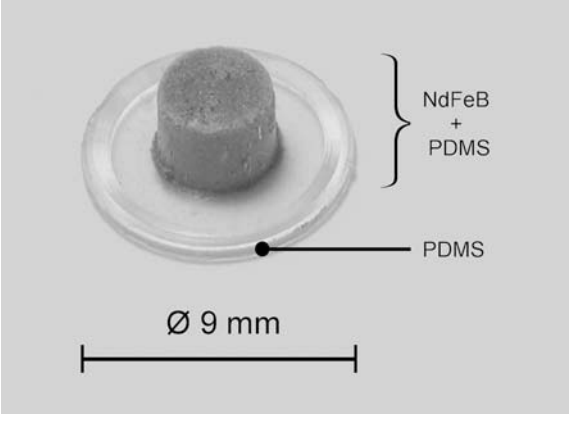

Fig. 5 Photograph of the magnetic membrane used for actuation of the micropump (external dimension Ø = 9 mm)

5 Characterization of the micropump

5.1 Magnetic membrane and electromagnet

The magnetic membrane was externally actuated by a 1,500-turn coil supplied with a sinusoidal current of

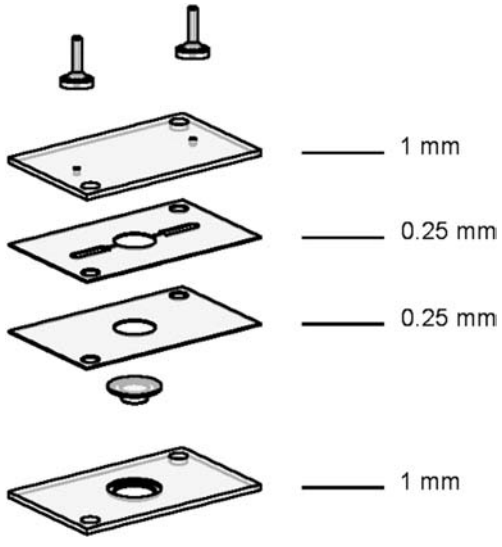

Fig. 6 Burst view of the complete device consisting of 4 PMMA layers with indicated thicknesses and an integrated PDMS magnetic membrane

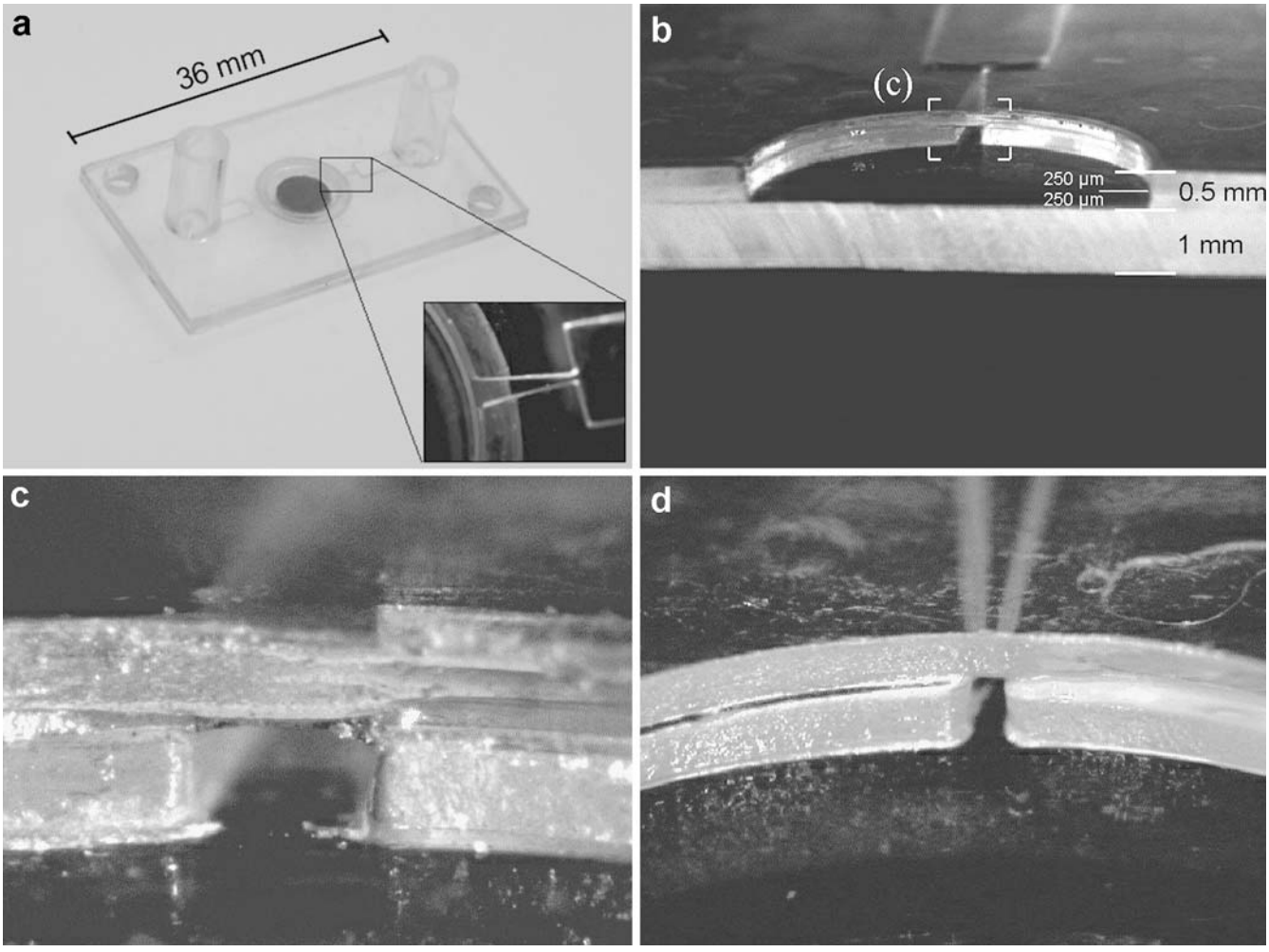

Fig. 7 **a** Photograph of the magnetic membrane actuated diffuser micropump; **b** cross-section of a partially assembled micropump; **c** zoom on the inlet diffuser; **d** zoom on the outlet diffuser

150 mA amplitude (see schematic diagram in the insert of Fig. 8a). The electromagnet has a soft magnetic iron core for magnetic field concentration. Figure 8a shows the magnetic induction along the symmetry line (z axis) of the electromagnet with and without the presence of the soft iron core, as measured by a Hall probe (Teslameter model 6010, F.W. Bell, Orlando, FL, USA). We clearly observe the amplification of the induction by a factor of about eight when using the soft core. Figure 8b shows the vertical gradient of the z component of the magnetic induction d B_z/d z, which is proportional to the actuation force. In an electromagnetic system consisting of a moving permanent magnet and a soft magnetic circuit the resulting force generally is composed of a positive contribution as a result of the magnetization of the soft material by the permanent magnet and a contribution as a result of the presence of the permanent magnet in the field of the electromagnet. This second type of force in the z direction for a permanent magnet with magnetization M_z and volume V is given by

$$F_z = M_z \int_V \frac{\mathrm{d}B_z}{\mathrm{d}z}\,\mathrm{d}V \tag{7}$$

We measured the magnetic induction generated by the permanent magnet membrane using a Hall probe and obtained a value of 0.09 T at the surface of the magnet. From this value we derived a z component of the magnetization $M_z \approx 1.44 \times 10^5$ A.m^{-1}, taking into account the demagnetization factor of the permanent magnet (~0.5), the polymer magnet being characterized by a diameter of 5 mm, a height of 2.2 mm and a volume of 4.3×10^{-8} m^3. We can now evaluate Eq. 7 considering the magnetic field generated by the electromagnet at the center of the polymer permanent magnet (see Fig. 8). For example, when the polymer magnet is in contact with the soft iron core of the electromagnet, its center position is at $z = 1$ mm providing a force of about 100 mN. During normal pumping operation the middle of the polymer magnet is 3 mm away from the soft iron core and the magnetic membrane deflection is not larger than 0.25 mm, giving a typical magnetic force of 75 mN. For a PDMS membrane area in contact with the liquid of 3.8×10^{-5} m^2 this corresponds to an effective actuation pressure of ~20 mbar. This value is of the same

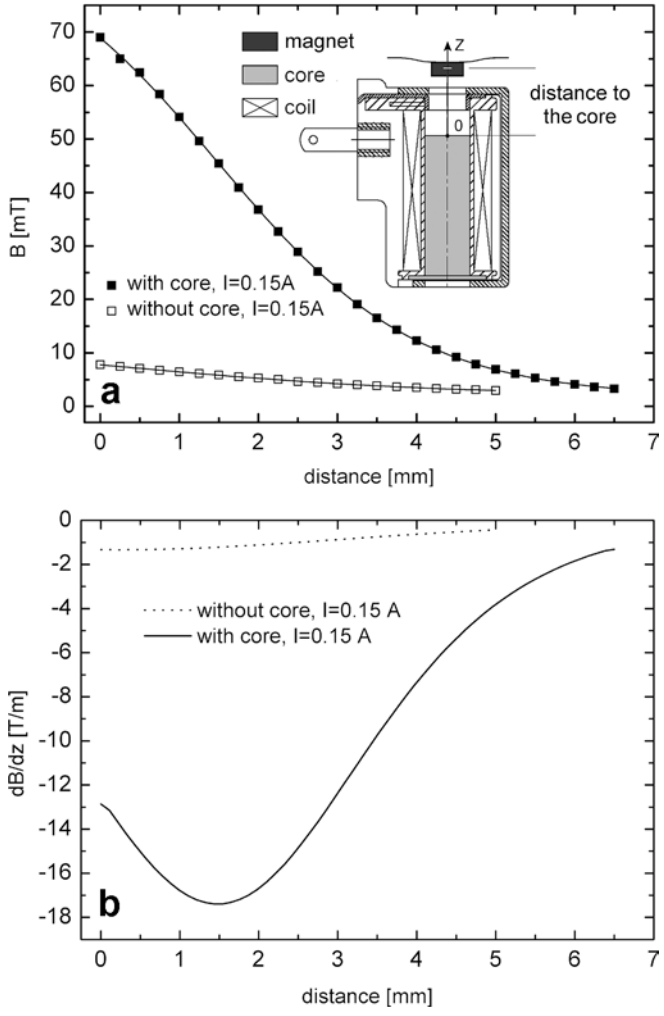

Fig. 8 Magnetic characteristics of the electromagnet with and without magnetic core: **a** magnetic induction along the symmetry line (z axis); **b** vertical gradient of the z component of the magnetic induction along the z axis

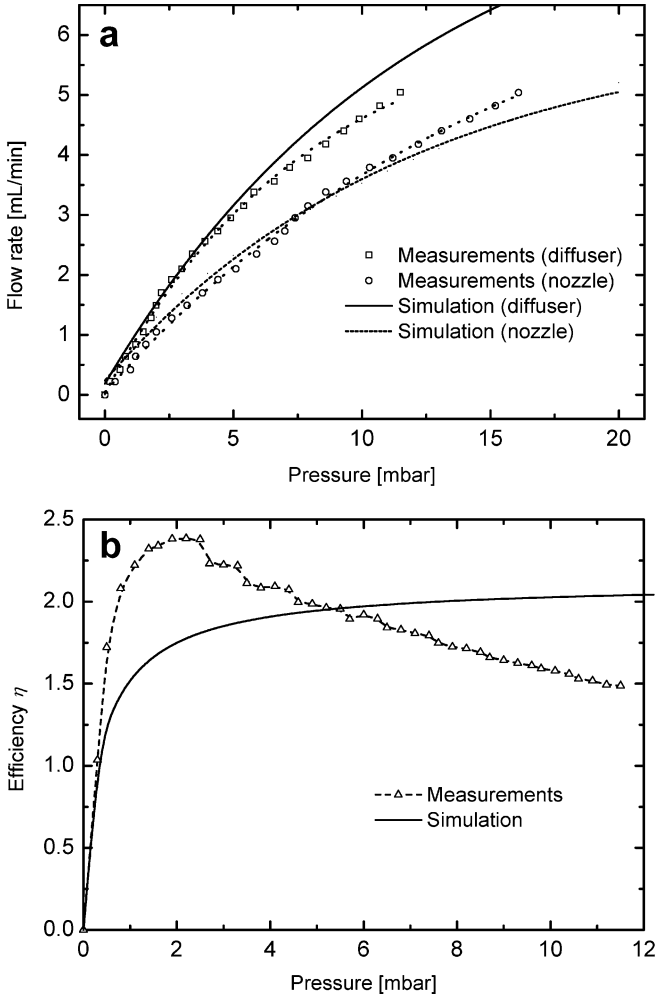

Fig. 9 **a** Flow rate–pressure measurement for a discrete nozzle/diffuser element, identicate to that used in the micropump, but with a thickness of 0.5 mm. **b** Plot of the efficiency vs. pressure calculated from the results of Fig. 9a using Eq. 5

order as the measured backpressure of the micropump (see further).

5.2 Diffuser

The performance of a single diffuser was tested in a separate device fabricated in metal by laser cutting. The dimensions are those given in the design and theory section, except for the thickness, which is 0.5 mm. Figure 9 shows the experimental flow rate of the structure in both the diffuser and nozzle direction, compared with a numerical simulation using Femlab 2.2 (Comsol). Comparing our experimental results with this simulation provides us with the value for the efficiency of the nozzle/diffuser element $\eta = (\phi_d/\phi_n)^2 \approx 2$, which is a factor of two smaller than the theoretical–empirical value derived above (Eq. 5) in the applied range of pressures. We draw the reader's attention to the fact that the empirical estimate of the diffuser efficiency relies on experiments that were done on diffuser–duct elements having a size in the range of centimeters.

5.3 Resonance frequency

The flow rate–backpressure dependence was measured with a water-filled glass tube, providing a hydrostatic backpressure ρgH, as illustrated in Fig. 10a. Besides water, we have pumped air with our micropump using the setup shown in Fig. 10b. The flow rate of air was determined from the time dependence of the air pocket in the chamber of Fig. 10b. The flow rate results against backpressure for water are shown in Fig. 11 for different membrane actuation frequencies. Compressibility aspects of air can be neglected for this range of pressures. In all cases, the flow rate decreased linearly with the backpressure, which is the expected behavior of a reciprocating pump (Zimmermann et al. 2004). Depending on the actuation frequency, we obtained a non-zero flow rate up to ~12 mbar, which is of the same

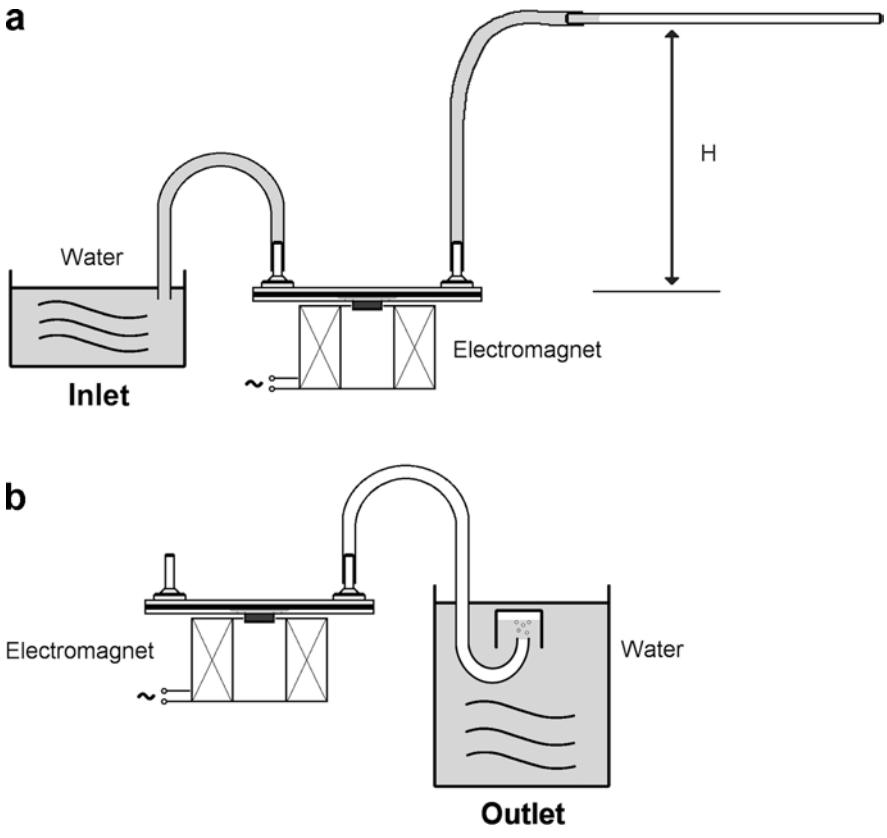

Fig. 10 Experimental setup used to measure the flow rate dependence **a** on backpressure and frequency for water; **b** on frequency for air

order as the pressure provided by the magnetic membrane.

For actuation frequencies close to the natural frequency of the system, we obtained membrane vibrations of larger amplitude that produce a higher flow rate of the pump. A comprehensive explanation of resonance phenomena in fluidic systems can be found in (Naudascher and Rockwell 1994). Figure 12 shows the flow rate-frequency dependence for the pumping of water without backpressure. A resonance frequency of ~12 Hz can be observed. For water pumping, the resonance frequency of a nozzle/diffuser reciprocating pump was theoretically calculated by Olsson et al. (1999). They used an energy analysis technique, where the total energy (not taking into account losses) oscillates between the maximum kinetic energy of the fluid in the nozzle/diffuser element and the maximum potential energy of the diaphragm. In their model, the resonance frequency of the pump is determined by the membrane stiffness and the inertia of the fluid in the diffusers:

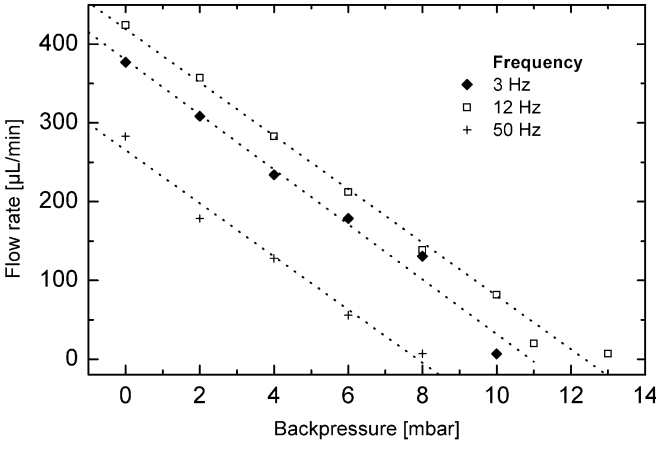

Fig. 11 Water flow–backpressure characteristics of the micropump for different excitation frequencies with *dotted trend lines*

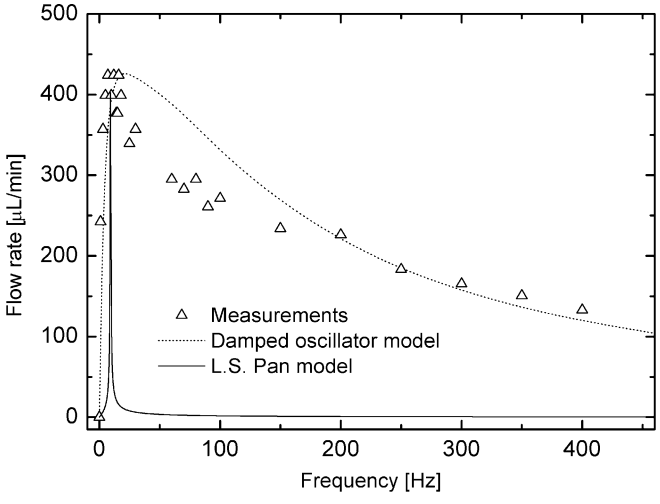

Fig. 12 Water flow rate for different excitation frequencies, without backpressure. The *dotted trend line* is calculated using the damped oscillator model of Eq. 18. The *solid line* is calculated using the model of Pan et al. (2003) (Eq. 14)

$$f_0 = \frac{1}{2\pi}\sqrt{\frac{K_p\left(1+\sqrt{\eta}\right)^2 h\,(w_2 - w_1)}{\rho\,K_v\,(1+\eta)\,L\,\ln\frac{w_2}{w_1}}} \tag{8}$$

By monitoring the membrane deflection as a function of pressure, the membrane stiffness was measured to be $K_p = 6$ MPa. K_v is the ratio of the pumping chamber volume variation amplitude to the deflection of the membrane at the center, which we estimated to be $1.96 \times 10^{-5}\ \mathrm{m}^2 < K_v < 3.85 \times 10^{-5}\ \mathrm{m}^2$. The resonance frequency calculated with Eq. 8 was estimated to be $14\ \mathrm{Hz} < f_0 < 20\ \mathrm{Hz}$ for water, which is in good agreement with the measured resonance frequency of 12 Hz (see Fig. 12). Note that the efficiency η, while important for giving a high flow rate, has a minor influence on the resonance frequency.

When pumping air, the inertia of the nozzle/diffuser element is of the same order as the membrane inertia, so that the latter can not be neglected. Figure 13 shows the flow rate-frequency dependence for the pumping of air without backpressure. A resonance frequency around 200–250 Hz can be observed. Pan et al. (2003) proposed the following formula for the resonance frequency of a diffuser micropump actuated with a thin membrane, which takes into account the inertia of both the membrane and the fluid in the pumping chamber and in the diffusers:

$$f_0 = \frac{f_1}{\sqrt{1 + R_p\left[\frac{D}{h} + \frac{\left(1+\alpha^2\right) L A_m}{2h\sqrt{A_1 A_2}}\right]}} \tag{9}$$

where A_m is the membrane surface, R_p is the ratio between the fluid density ρ and the equivalent membrane density $\rho_m = M_m/(A_m h)$. The resonance frequency of the membrane f_1 is determined by its elastic constant and mass M_m:

$$f_1 = \frac{1}{2\pi}\sqrt{\frac{K_p\,A_m}{M_m}} \tag{10}$$

The pump stroke efficiency α is calculated from Eqs. 3 and 4:

$$\alpha = \frac{\sqrt{\xi_n} - \sqrt{\xi_d}}{\sqrt{\xi_n} + \sqrt{\xi_d}} = \frac{\sqrt{\eta} - 1}{\sqrt{\eta} + 1} \tag{11}$$

From Eq. 11, we find that:

$$\frac{1+\alpha^2}{2} = \frac{1+\eta}{\left(1+\sqrt{\eta}\right)^2} \tag{12}$$

For $R_p \gg 1$, and neglecting the inertia of the fluid in the chamber (term D/h), Eq. 9 can be rewritten as:

$$f_0 = \frac{f_1}{\sqrt{R_p\left[\frac{\left(1+\alpha^2\right) L A_m}{2h\sqrt{A_1 A_2}}\right]}} \tag{13}$$

Using Eqs. 10 and 12, one finds that Eqs. 8 and 13 are equivalent, demonstrating that Eq. 8 is a particular case of Eq. 9. Putting in the various parameters into Eqs. 9 and 10, with $\rho = 1.3\ \mathrm{kg\ m^{-3}}$ for air, we find that the membrane resonance frequency $f_1 \sim 200$ Hz, and the experimental pumping resonance frequency for air $f_0 \sim 180$ Hz is close to this frequency (see Fig. 13).

5.4 Frequency-dependent flow rate

Besides the resonance frequency, Pan et al. (2003) also calculated the frequency-dependent flow rate, taking into account energy losses in the nozzle/diffuser elements, but not in the microfluidic channel or in the membrane. In the simplest case, where there is no pressure difference between the inlet and the outlet, they found for the flow rate Q:

$$Q = \frac{\alpha \bar{F}}{\pi}\sqrt{\frac{6\pi C_1}{\sqrt{\left(16\beta C_3 \bar{F}\right)^2 + 9\pi^2(1-C)^4} + 3\pi(1-C)^2}} \tag{14}$$

with $\bar{F}$ the dimensionless actuation force, $C = (\omega/\omega_o)^2$, $C_1 = (\omega/\omega_1)^2$,

$$C_3 = \frac{R_p\,C_1}{8}\left(\frac{A_m}{A_1}\right)^2,$$

and

$$\beta = \frac{2\,\xi_n\,\xi_d}{\left(\sqrt{\xi_n} + \sqrt{\xi_d}\right)^2}$$

with $\omega = 2\pi f$, $\omega_0 = 2\pi f_0$ and $\omega_1 = 2\pi f_1$. This equation corresponds to Eq. 42 of Pan et al. (2003). We have

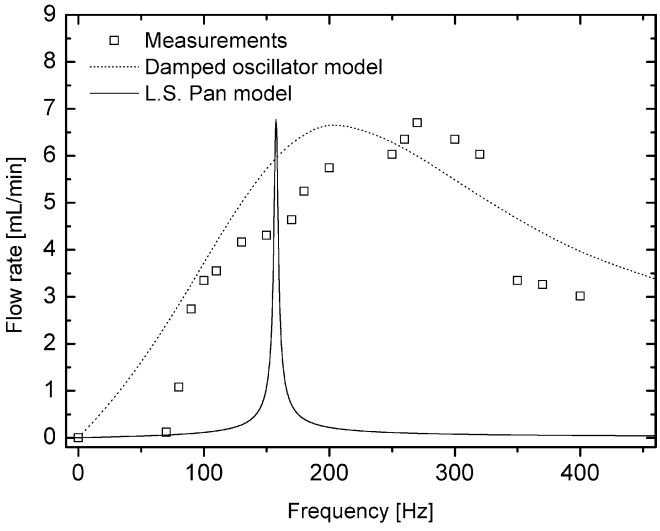

Fig. 13 Air flow rate for different excitation frequencies, without backpressure. The *dotted trend line* is calculated using the damped oscillator model of Eq. 18. The *solid line* is calculated using the model of Pan et al. (2003) (Eq. 14)

fitted our experimental data for both water and air pumping with no adjustable fitting parameters, except for the dimensionless force $\bar{F}$, in such a way that the experimental and theoretical flow rates coincide at resonance. The results are presented in Figs. 12 and 13. For both cases, the theory of Pan et al. (2003) predicts a very narrow resonance peak besause of an underestimation of the losses in the fluidic circuit. In the case of a forced oscillating system with damping the dependence of the membrane deflection amplitude X on pulsation ω is given by Naudascher and Rockwell (1994):

$$X = \frac{\delta_{\text{static}}}{\sqrt{\left(2\,\xi\,\frac{\omega}{\omega_0}\right)^2 + \left(1 - \left(\frac{\omega}{\omega_0}\right)^2\right)^2}} \tag{15}$$

with ξ a dimensionless damping coefficient, and δ_{static} the average static deflection of the membrane for the applied force F, which can be written as:

$$\delta_{\text{static}} = \frac{F}{K_{\text{p}}\,A_{\text{m}}} \tag{16}$$

The flow rate of the pump Q can be estimated from the average membrane deflection amplitude X times the pulsation ω, corrected by the pump stroke efficiency α, giving the following equation:

$$Q \approx \frac{\alpha}{\pi}\,A_{\text{m}}\,X\,\omega \tag{17}$$

Rewriting Eq. 17 results in:

$$Q \approx \frac{\alpha}{\pi}\,A_{\text{m}}\,\delta_{\text{static}}\,\omega_1 \sqrt{\frac{\left(\frac{\omega}{\omega_1}\right)^2}{\left(2\,\xi\,\frac{\omega}{\omega_0}\right)^2 + \left(1 - \left(\frac{\omega}{\omega_0}\right)^2\right)^2}} \tag{18}$$

For our micropump, losses take place in the diffusers, in the channels, and in the membrane. These multiple sources complicate the estimation of the parameter ξ. The following values were used for the fitting curve of Fig. 12: $\alpha = 0.2$, $\delta_{\text{static}} = 170$ µm, $\xi = 35$, $f_{\text{o}} = 12$ Hz, $f_1 = 200$ Hz; while for the curve of Fig. 13, we find that $\alpha = 0.2$, $\delta_{\text{static}} = 55$ µm, $\xi = 0.7$, $f_{\text{o}} = 180$ Hz, $f_1 = 200$ Hz, in good agreement with the geometrical parameters of the micropump. We note that the damping effect is more important for water than for air, which can be related to the higher dynamic viscosity of water ($\mu_{\text{water}} = 1.0 \times 10^{-3}$ Ns/m^2 at 20°C) compared to air ($\mu_{\text{air}} = 1.8 \times 10^{-5}$ Ns/m^2 at 20°C). For comparison, if we fit the theoretical curves of Pan et al. (2003) with the damped forced oscillator model, we find for the dimensionless loss coefficient $\xi = 0.35$ and 0.007 for water and air, respectively. Our experiments are the first ones that directly demonstrate the damped resonance behavior of a nozzle/diffuser micropump. Although resonance frequencies are correctly predicted by the models of Olsson et al. (1999) and Pan et al. (2003), the damping behavior is strongly underestimated in the theory of Pan. Indeed, to correctly fit our experimental data, the losses in the theory of Pan need to be overestimated by a factor 100. A possible explanation for the discrepancy between our experimental data and the model of Pan et al. (2003) might be the importance of losses in the complete microfluidic circuit (and not only in the nozzle/diffuser elements), in particular losses caused by squeezed film damping in our pumping chamber, which has a vertical dimension of the order of the membrane deflection amplitude.

6 Conclusion and outlook

We have designed and experimentally realized nozzle/diffuser structures for application in a PMMA micropump. The combination of the nozzle/diffuser elements with an electromagnetically actuated PDMS membrane, characterized by a large deflection amplitude, resulted in a self-priming micropump with which we successfully pumped both water and air. Its flow rate–backpressure performance has been characterized and the micropump resonance frequency showed good agreement with the theoretical models of Olsson et al. (1999) and Pan et al. (2003). The frequency-dependent flow rate can be well understood by a fluidic damped oscillator model. Our results indicate that electromagnetic actuation is a simple actuation method that presents a serious alternative to piezoelectric actuation. In particular, we anticipate that the technology presented above can be advantageously applied for lab-on-a-chip applications where low cost and/or disposable aspects are of primary importance. Future developments include an enhancement of the maximum operation pressure by increasing the volume of the magnet, by using powders with improved magnetic characteristics or by creating an electromagnetic actuation circuit with higher effective permeability.

Acknowledgements The authors gratefully acknowledge the Swiss Commission for Technology and Innovation for financially supporting this project (Project CTI-Medtech 4960.1 MTS) and Dr D. Solignac and Dr A. Donzel for useful discussions.

References

Accoto D, Carrozza MC, Dario P (2000) Modelling of micropumps using unimorph piezoelectric actuator and ball valves. J Micromech Microeng 10:277–281

Beebe DJ, Moore JS, Bauer JM, Yu Q, Liu RH, Devadoss C, Jo BH (2000) Functional hydrogel structures for autonomous flow control inside microfluidic channels. Nature 404:588–590

Blevins RD (1984) Applied fluid dynamics handbook. Van Nostrand-Reinhold, New York

Böhm S, Olthuis W, Bergveld P (1999) A plastic micropump constructed with conventional techniques and materials. Sens Actuators A, Phys 77:223–228

Cho HJ, Ahn CH (2003) Microscale resin-bonded permanent magnets for magnetic micro-electro-mechanical systems applications. J Appl Phys 93:8674–8676

Cockrell DJ, Markland E (1963) A review of incompressible diffuser flow. Aircraft Eng 35:286–292
Forster F, Bardell R, Afromowitz M, Sharma N (1995) Design, fabrication and testing of fixed-valve micropumps. In: Proceedings of the ASME Fluids Engineering Division, International Mechanical Engineering Congress and Exposition, San Francisco, USA, pp 39–44
Gerlach T (1998) Microdiffusers as dynamic passive valves for micropump applications. Sens Actuators A, Phys 69:181–191
Gerlach T, Schuenemann M, Wurmus H (1995) A new micropump principle of the reciprocating type using pyramidic micro flowchannels as passive valves. J Micromech Microeng 5:199–201
Gibson AH (1945) Hydraulics and its applications. Constable, London, p 93
Greivell N, Hannaford B (1997) The design of a ferrofluid magnetic pipette. IEEE Trans Biomed Eng 44:129–135
Hatch A, Kamholz AE, Holman G, Yager P, Bohringer KF (2001) A ferrofluidic magnetic micropump. J Microelectromech Syst 10:215–221
Khoo M, Liu C (2000) A novel micromachined magnetic membrane microfluid pump. In: International Conference of the IEEE Engineering in Medicine and Biology Society (EMB), Chicago, IL
Lagorce LK, Brand O, Allen MG (1999) Magnetic microactuators based on polymer magnets. J Microelectromech Syst 8:2–9
Liu C (1998) Development of surface micromachined magnetic actuators using electroplated permalloy. J Mechatronics 613–633
Manz A, Fettinger JC, Verpoorte E, Ludi H, Widmer HM, Harrison DJ (1991) Micromachining of monocrystalline silicon and glass for chemical analysis systems—a look into next century's technology or just a fashionable craze? Trends Anal Chem 10:144–149
Manz A, Graber N, Widmer HM (1990) Miniaturized total chemical analysis systems: a novel concept for chemical sensing. Sens Actuators B, Chem 1:244–248
Morris CJ, Forster FK (2003) Low-order modeling of resonance for fixed-valve micropumps based on first principles. J Microelectromech Syst 12:325–334
Naudascher E, Rockwell D (1994) Flow-induced vibrations: an engineering guide. Balkema, Brookfield, USA
Nguyen N-T, Huang X (2001) Miniature valveless pumps based on printed circuit board technique. Sens Actuators A, Phys 88:104–111
Nguyen N-T, Huang XY, Chuan TK (2002) MEMS-micropumps: a review. J Fluids Eng 124:384–392
Nguyen N-T, Truong T-Q (2004) A fully polymeric micropump with piezoelectric actuator. Sens Actuators B, Chem 97:139–145
Olsson A (1998) Valve-less diffuser micropumps. PhD thesis, Royal Institute of Technology, Stockholm, Sweden
Olsson A, Enoksson P, Stemme G, Stemme E (1995) A valve-less planar pump in silicon. In: Proceeding of the 8th IEEE International Conference on Transducers, Stockholm, Sweden, vol 2, pp 291–294
Olsson A, Larsson O, Holm J, Lundbladh L, Ohman O, Stemme G (1998) Valve-less diffuser micropumps fabricated using thermoplastic replication. Sens Actuators A, Phys, 64:63–68
Olsson A, Stemme G, Stemme E (1996) Diffuser-element design investigation for valve-less pumps. Sens Actuators A, Phys 57:137–143
Olsson A, Stemme G, Stemme E (1999) A numerical design study of the valveless diffuser pump using a lumped-mass model. J Micromech Microeng 9:34–44
Pan LS, Ng TY, Wu XH, Lee HP (2003) Analysis of valveless micropumps with inertial effects. J Micromech Microeng 13:390–399
Patterson GN (1938) Modern diffuser design. Aircraft Eng 10:267
Richter M, Linnemann R, Woias P (1998) Robust design of gas and liquid micropumps. Sens Actuators A, Phys 68:480–486
Santra S, Holloway P, Batich CD (2002) Fabrication and testing of a magnetically actuated micropump. Sens Actuators B, Chem 87:358–364
Singhal V, Garimella SV, Murthy JY (2004) Low Reynolds number flow through nozzle-diffuser elements in valveless micropumps. Sens Actuators (in press)
Stemme E, Stemme G (1993) A valveless diffuser/nozzle-based fluid pump. Sens Actuators A, Phys 39:159–167
Tay FEH, Choong WO (2002) Literature review for micropumps. In: Tay FEH (ed) Microfluidics and BioMEMS applications. Kluwer, Boston, MA
Van de Pol FCM, Van Lintel HTG (1990) A thermopneumatic micropump based on micro-engineering techniques. Sens Actuators A, Phys 21:198–202
Van Lintel HTG, Van de Pol FCM, Bouwstra S (1988) A piezoelectric micropump based on micromachining of silicon. Sens Actuators 15:153–167
White FM (1998) Fluid mechanics, 4th edn. McGraw-Hill, New York
Yamahata C, Chastellain M, Parashar VK, Petri A, Hofmann H, Gijs MAM (2004) Plastic micropump with ferrofluidic actuation. J Microelectromech Syst (in press)
Yamahata C, Gijs MAM (2004) Plastic micropumps using ferrofluid and magnetic membrane actuation. In: Proceeding of the 17th IEEE International Conference on Micro electro mechanical systems, Maastricht, The Netherlands, pp 458–461
Zhang W, Ahn CH (1996) A bi-directional magnetic micropump on a silicon wafer. Paper presented at the "Solid-state sensor and actuator workshop", Hilton Head Island, SC, USA
Zimmermann S, Frank LA, Liepmann D, Pisano AP (2004) A planar micropump utilizing thermopneumatic actuation and in-plane flap valves. In: Proceeding of the 17th IEEE International Conference on Micro electro mechanical systems, Maastricht, The Netherlands, pp 462–465